



Design and synthesis of an AIE-active fluorogen with red emission and its biological application

Lufei Xiao¹ · Hongji Sun³ · Le Zhou² · Di Li² · Hui Wang²

Received: 26 January 2018 / Accepted: 6 June 2018 / Published online: 9 June 2018
© Institute of Chemistry, Slovak Academy of Sciences 2018

Abstract

A novel triphenylamine-base derivative **L** containing pyridine and terpyridine was designed and synthesized. Compound **L** exhibited distinct aggregation-induced emission (AIE) behavior in water–ethanol and also displayed a threefold increase in the intensity of luminescence at 608 nm. Furthermore, confocal microscopy imaging demonstrated that compound **L** displays low toxicity and brights red fluorescence in mitochondria in living HepG2 cells. Inherent from the mitochondrial-targeting ability of pyridine moiety and the AIE characteristic of triphenylamine group, compound **L** could be employed as a fluorescent probe in the near-infrared region for living cell imaging.

Keywords Aggregation-induced enhanced emission · Triphenylamine · Mitochondria · Pyridine

Introduction

Fluorescent organic materials have attracted increasing interest due to their potential applications in bioimaging and chemosensing (Zhang et al. 2017; Huang et al. 2016; Chang et al. 2016). However, a majority of fluorescence organic materials face the problem of aggregation-induced quenching (ACQ) because of strong π – π stacking interactions in the enlarged π -conjugated system (Thomas et al. 2007), resulting in limitation of their practical applications. Aggregation-induced emission (AIE), as a novel phenomenon, was first discovered by Tang's group (Luo et al. 2001).

The compound exhibits very weak fluorescence in solution but emits strong fluorescence in the aggregated state. Currently, AIE materials have gained widespread attentions for their potential application in various fields, for instance bioimaging, chemosensors and organic light-emitting diodes (Gui et al. 2017; Mei et al. 2015). However, the working mechanism of the AIE processes is very complicated, and the reason is still unclear. At present, some theories or hypotheses are proposed to explain the AIE phenomenon, e.g., intramolecular restrictions, J-type aggregates, restriction of intramolecular rotation, twisted intramolecular charge transfer (Li et al. 2017a; Kwork et al. 2015; Ding et al. 2013). Therefore, a large number of compounds with AIE properties have been developed. To further enlarge the family of specific AIE-active compounds, it is necessary to carry out more extensive investigations in this field.

Herein, we developed a novel A–D– π –A type triphenylamine-based derivative (Fig. 1), which displays AIE behavior in water–ethanol system. First, triphenylamine moiety with a strong electron donor can help to delocalize the electron distribution and extend the conjugation system (Liu et al. 2014). Second, owing to the strong electron-withdrawing ability and large π -conjugation system, terpyridine ligand exhibits good optical properties (Wang et al. 2018a). Third, the pyridinium cation moiety with high membrane potential is able to target intracellular mitochondria (Tian et al. 2017). Compound **L** displays good AIE characteristic and emits red fluorescence.

Electronic supplementary material The online version of this article (<https://doi.org/10.1007/s11696-018-0529-0>) contains supplementary material, which is available to authorized users.

✉ Lufei Xiao
xlf3345@163.com

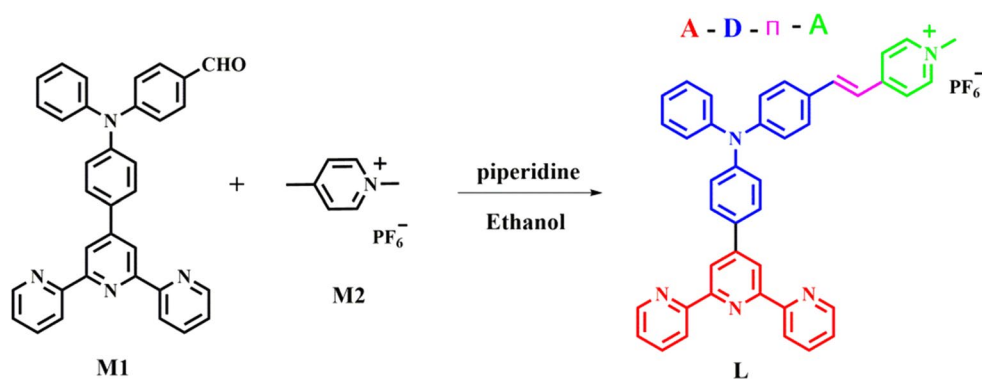
✉ Hui Wang
wanghias@126.com

¹ Department of Food and Environmental Engineering, Chuzhou Vocational and Technical College, Chuzhou 239000, People's Republic of China

² Department of Chemistry, Wannan Medical College, Wuhu 241002, People's Republic of China

³ Anhui Province Key Laboratory of Active Biological Macro-molecules Research, Wannan Medical College, Wuhu 241002, People's Republic of China

Fig. 1 Synthesis of the compound **L**



As expected, compound **L** is capable of targeting mitochondria.

Experimental section

Materials and measurements

All of the reagents were available commercially and used without further purification. ^1H NMR and ^{13}C NMR spectra were obtained on Bruker 400 Ultrashield spectrometer. Mass spectrum was measured on HRMS-LTQ Orbitrap XL (ESI source). IR spectra (KBr pressed pellets) were obtained on Nicolet FT-IR-870SX spectrophotometer. UV–Vis absorption and one-photon fluorescence spectra were obtained on UV-1700 and Hitachi F-4600 fluorescence spectrophotometer, respectively.

Synthesis of **L**

M1 (Wang et al. 2016) (0.50 g, 1 mmol) were dissolved in ethanol (50 mL), **M2** (Tian et al. 2017) (0.25 g, 1 mmol) and 3 drops piperidine were subsequently added. The reaction mixture was refluxed for 24 h. The solid was filtered off and washed with ethanol. The product was recrystallized from methanol to afford red solids. IR (cm^{-1}) selected bands: 2918, 2135, 1796, 1646, 1585, 1510, 1468, 1439, 1418, 1389, 1323, 1292, 1175, 972, 875, 841, 793, 699, 660, 621, 557, 540. ^1H NMR (d_6 -DMSO) δ : 8.77 (m, 4 H), 8.70 (m, 4 H), 8.16 (d, $J = 6.9$ Hz, 2 H), 8.05 (t, $J = 7.8$ Hz, 2 H), 7.97 (m, 3 H), 7.69 (d, $J = 8.7$ Hz, 2 H), 7.54 (m, 2 H), 7.44 (t, $J = 7.9$ Hz, 2 H), 7.36 (d, $J = 16.2$ Hz, 1 H), 7.23 (m, 5 H), 7.12 (d, $J = 8.7$ Hz, 2 H), 4.23 (s, 3 H). ^{13}C NMR (d_6 -DMSO) δ : 156.1, 155.4, 149.7, 145.2, 140.7, 137.9, 130.4, 130.1, 128.6, 126.2, 125.4, 124.9, 124.8, 123.4, 122.7, 121.5, 121.3, 117.7, 56.4. MS: 594.26 ($[\text{M}-\text{PF}_6]^+$).

Computational details

The ground state geometries of the molecules are optimized at the time-dependent density functional theory (TD-DFT)/CAM-B3LYP (Yannai et al. 2004) functional level without any symmetry restraint (Wang et al. 2012) using Gaussian 09 program (Frisch et al. 2009). The UV–Vis absorption properties are obtained based on the optimized structures with CAM-B3LYP functional utilizing Gaussian 09 package. The basis set of 6-31G* is chosen for all atoms. An analytical frequency confirms evidence that the calculated species represents a true minimum without imaginary frequencies on the respective potential energy surface. The lowest 25 spin-allowed singlet–singlet transitions, up to energy of about 5 eV, were taken into account in the calculation of the absorption spectra. The molecular orbitals were visualized using GaussView 5.0.9 (Dennington et al. 2009).

Results and discussion

Photophysical properties

The UV–Vis absorption and one-photon fluorescence spectra of **L** in different polar solvents were initially investigated. The corresponding photophysical data were summarized in Table 1. As depicted in Fig. 2, compound **L** exhibited two strong absorption bands at about 460 nm and 275 nm in different solvents, which can be assigned to the π – π^* transition mixed with intramolecular charge transfer process (ICT) and $\pi_{\text{terpyridine}}-\pi_{\text{terpyridine}}^*$ transition, respectively. Weak solvatochromism was observed in the maximum absorption band, indicative of the little difference in dipoles between the ground and the excited states of the compound. Increasing the solvent polarity from benzene to DMF (Fig. 2 and Table 1), the fluorescence maxima of **L** shifted from 593 to 608 nm and the fluorescence was quenched at the same time, which might be assigned to ICT. Moreover, the Stokes' shifts also exhibited an increasing tendency with the increase of

Table 1 The photophysical data of **L** in different solvents

Solvents	$\lambda_{\max}^{\text{abs}}$ (nm) ^a	$\epsilon_{\max}^{\text{b}}$	$\lambda_{\max}^{\text{SPEF}}$ (nm) ^c	$\Delta\nu$ (nm) ^d	Φ^{e}
Benzene	477	3.40	594	117	0.28
Tetrahydrofuran	472	3.62	607	135	0.10
Ethyl acetate	460	3.56	604	144	0.14
Ethanol	472	3.61	604	132	0.06
Acetonitrile	461	3.22	604	143	0.009
DMF	460	3.07	608	148	0.02

^aPeak position of the larger absorption band^bMolar absorbance in $10^4 \text{ mol}^{-1} \text{ L cm}^{-1}$ ^cPeak position of one-photon fluorescence spectra, excitation at the absorption maximum^dStokes' shift in nm^eQuantum yields determined by using fluorescein as standard

the solvent polarity. To better understand the ICT process, we performed theoretical calculations with the density functional of CAM-B3lyp/6-31 g(d) (Fig. 3 and Table 2). From Fig. 3, the electron cloud of the highest occupied molecular orbital (HOMO) was dominated by the triphenylamine unit,

–C=C– moiety and pyridine unit. Meanwhile, the lowest unoccupied molecular orbital (LUMO) was localized on the pyridine group due to the strong electron-withdrawing ability. Due to the HOMO → LUMO transition, the absorption band at 484 nm was assigned as the ICT transition mixed with π – π^* transition, keeping consistent with the experimental ones.

Aggregation-induced emission (AIE) properties

Compound **L** could be dissolved in many organic solvents, such as THF, ethanol, acetonitrile and DMSO, but has poor solubility in water. To determine whether **L** is AIE active and considering the biological application, the UV–Vis absorption and fluorescence spectra of **L** in water–ethanol mixtures with different fraction of water (f_w) were investigated. From Fig. 4, we can see that compound **L** displayed three absorption bands in dilute ethanol solution. As the water fraction increased to 90%, the band at about 460 nm gradually decreased, accompanying with slightly blue shift. Moreover, the absorption curves decayed further from zero in the long wavelength region with high water fraction, indicating the existence of aggregative species in these solutions.

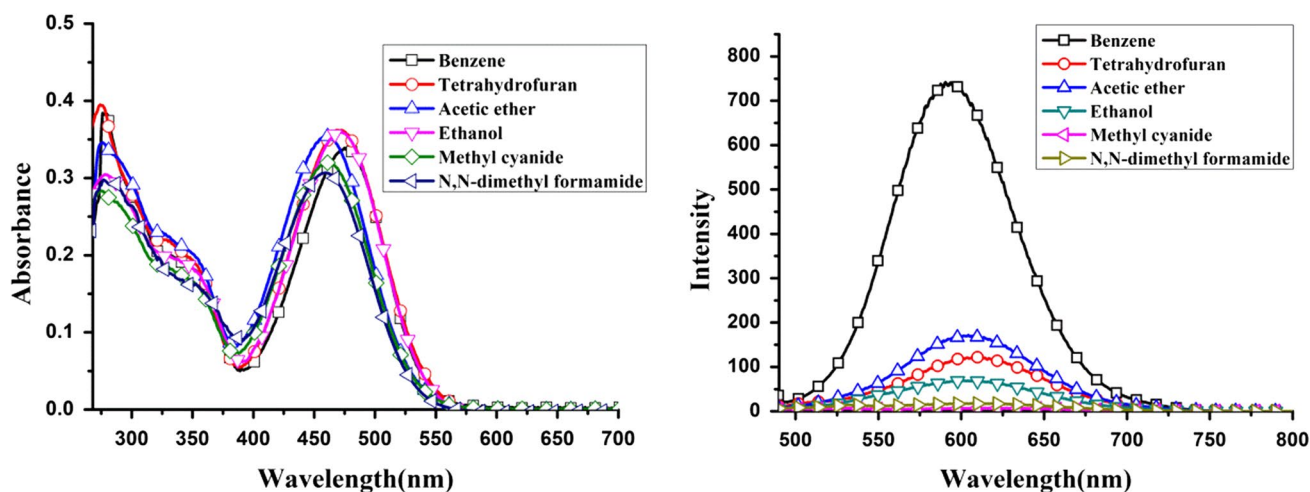
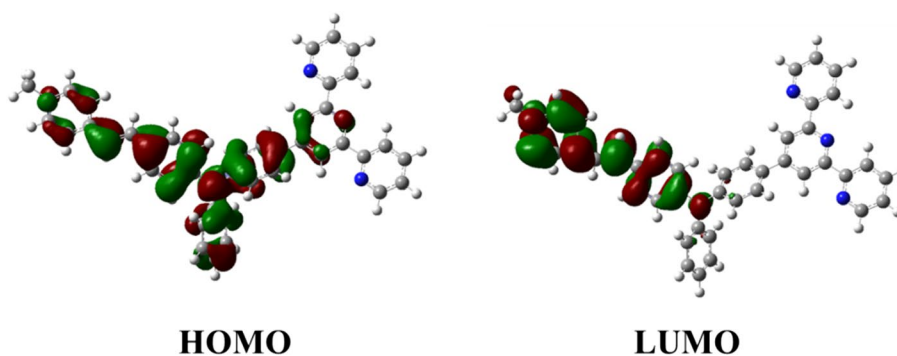
**Fig. 2** UV-Vis absorption (left) and one-photon fluorescence (right) spectra of **L** in different solvents**Fig. 3** Electron density distributions of frontier molecular orbitals of **L**

Table 2 Calculated linear absorption properties (nm), excitation energy (eV), oscillator strengths and major contribution for **L** using CAM-B3LYP/6-31G*

ΔE_1^a	λ (nm) ^b	Oscillator strengths	Nature of the transition
2.56	484	1.6598	156(H) → 157(L)(0.67)

^aThe energy gap of the electronic absorption band

^bPeak position of the maximum absorption band

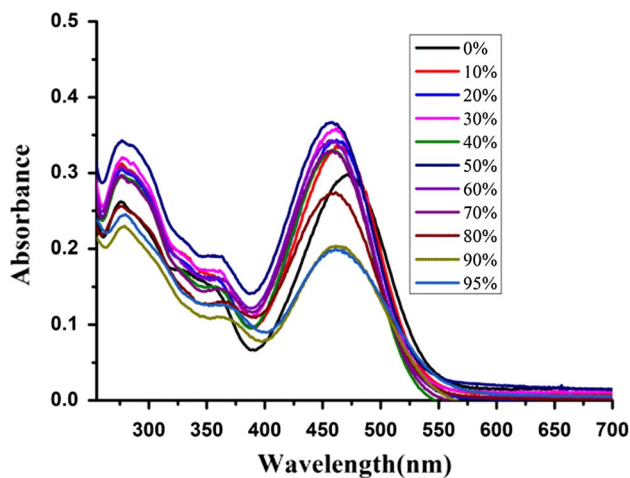


Fig. 4 UV-Vis absorption spectra of **L** in H₂O/ethanol mixtures with different fractions of water

Figure 5 exhibited the changes of fluorescence intensity of **L** in aqueous mixtures. In dilute ethanol solution, compound **L** was nearly non-emissive. The fluorescence intensity of **L** obviously decreased with the gradual addition of water amounts into ethanol solution. This phenomenon

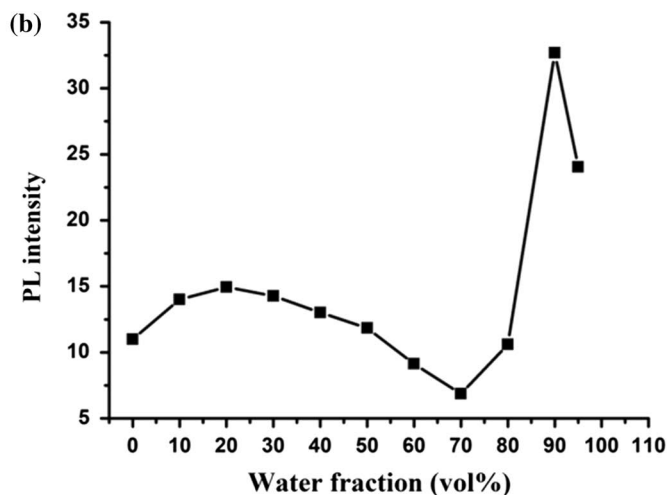
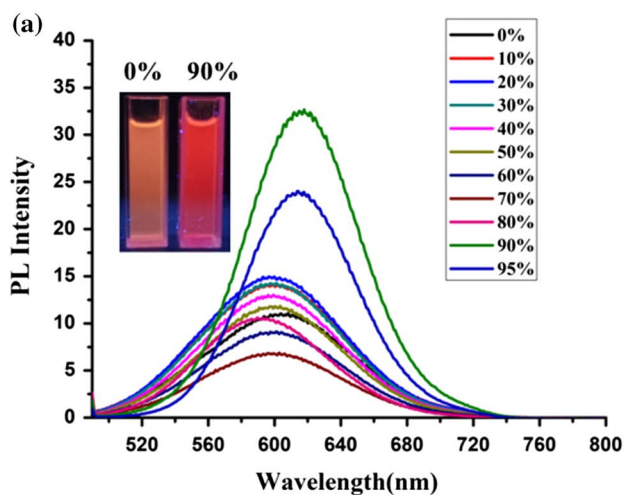


Fig. 5 **a** Emission spectra of **L** in H₂O/ethanol mixtures with different fractions of water, inset: photographs of **L** in H₂O/ethanol taken under 365 nm UV illumination. **b** The changes of fluorescence intensity with different water fractions

could be reasonably explained by a twisted intramolecular charge transfer (TICT) mechanism. The fluorescence intensity was invigorated at $f_w = 80\%$ and reached the maximum fluorescence intensity with $\lambda = 618$ nm at $f_w = 90\%$, which was a threefold enhancement to that of **L** in absolute ethanol solution, demonstrating the AIE characteristic of compound **L**. In this stage, compound **L** begins to aggregate because the solvating power of the aqueous mixture decrease, making the emission enhanced due to the restriction of intramolecular rotation effect. Meanwhile, the ICT effect is efficiently weakened. As depicted in Fig. 5b, when f_w reached 95%, the fluorescence intensity of **L** in the water–ethanol mixture decreased. This phenomenon has often been detected in some dyes possessing AIE properties, but the reason is still unclear. Up to now, this phenomenon could be explained by two possible factors: (1) in the extensive aggregation state, the molecules on the nanoparticle surface contributes mainly to the emission, while the molecules in interior contributes faintly, resulting in a decrease of fluorescence intensity. (2) When adding water to the solution, the molecules could form amorphous particles and crystal particles. The former one could decrease the fluorescence intensity, while the latter will enhance the intensity of fluorescence (Zheng et al. 2013).

To further explore the enhanced emission of **L** in water–ethanol system, the aggregate process of **L** with different water fractions was investigated by scanning electron microscopy (SEM). As shown in Fig. 6a, a spherical particle of **L** formed immediately in the mixture of water–ethanol with f_w of 40%. However, when $f_w = 90\%$, the AIE dots dispersed regularly and taken a block-like arrangement. These data demonstrated that the enhanced emission of **L** relies on the formation of nanoparticles. The comparative analysis of **L** with the previously reported AIE molecule was

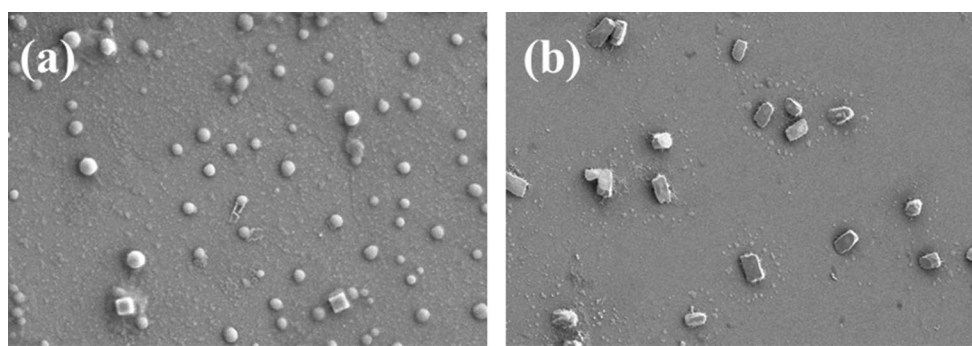


Fig. 6 SEM images of **L** in H₂O/ethanol mixtures with different water fractions: **a** H₂O/ethanol (40:60, v/v); **b** H₂O/ethanol (90:10, v/v)

Table 3 Comparison of the properties of **L** with the previously reported AIE molecule

Compound	Operating environment	Maximum emission wavelength (nm)	References
AIE-mito-TPP	DMSO/water	505	Hu et al. (2014)
TTE	THF/water (1:99, v/v)	410	Viglianti et al. (2017)
OPD-TPE-2CN	THF/water (8:92, v/v)	475	Xie et al. (2017)
1	DMF/water (10:90, v/v)	514	Wang et al. (2018b)
AIE-SRS-Mito	DMSO/water (1:99, v/v)	530	Li et al. (2017b)
5	THF/water (5:95, v/v)	676	Lu et al. (2016)
L	Ethanol/water (10:90, v/v)	618	This work

summarized in Table 3. Compared with the other reported AIE molecule, compound **L** exhibited long emission wavelength (> 600 nm), which encouraged us to explore its potential application in biological imaging.

Biological application

High cell viability is essential for a fluorescent probe in its biological application. To evaluate the cytotoxicity of **L**, HepG2 cells were treated with **L**, and its viability was subsequently determined by MTT assay. Figure 7 revealed that HepG2 cells incubated with 15 μM of **L** remained 90% viable after 24 h of feeding time, suggesting the low toxicity and good biocompatibility of **L**. To assess the cellular uptake properties, HepG2 cell was used as a model, whereby 10 μM of **L** was treated for 30 min followed by confocal microscopy imaging after washing with PBS. As shown in Fig. 8a, **L** could penetrate into the cell cytosol within the short incubation period and exhibited intensive red fluorescence. It is well-known that fluorophores possessing a pyridinium moiety can function as mitochondria probes. A co-staining experiment with Mitotracker deep red was performed to establish whether **L** could be internalized with membrane-rich mitochondria. As displayed in Fig. 8a, a clear mitochondria profile with strong green fluorescence was observed from the green channel, which was ascribed to Mitotracker deep red. A similar

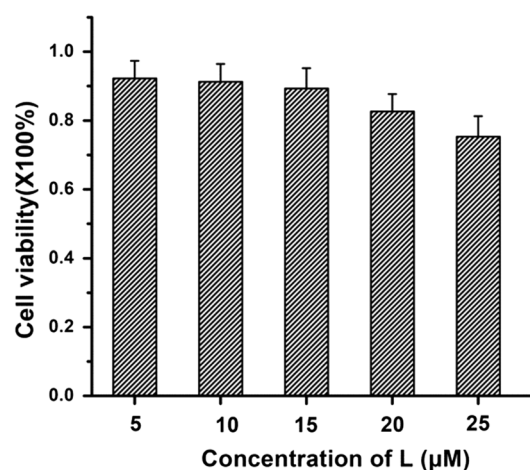


Fig. 7 Cytotoxicity data results obtained from the MTT assay at different concentrations for 24 h

mitochondria profile with red fluorescence was obtained after treating with **L**. The signal of **L** overlaid very well with the fluorescence of Mitotracker deep red (Fig. 8c). Moreover, Pearson's co-localization coefficient, which describes the correlation of the intensity distribution between these two channels, was calculated to be 0.92 (Fig. 8b), indicating compound **L** could selectively accumulate into the mitochondria. The above results revealed

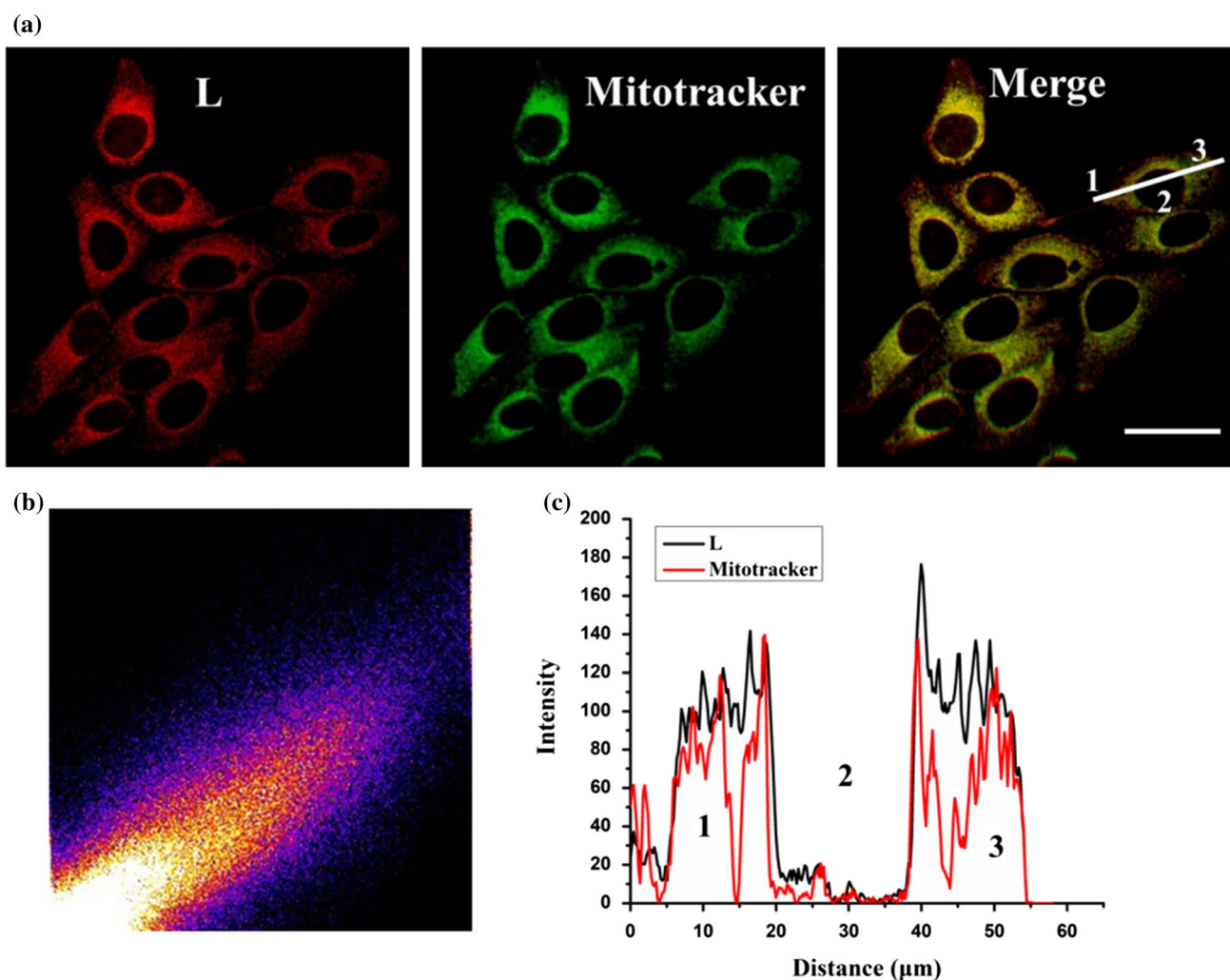


Fig. 8 Colocalization fluorescence microscopy images of HepG2 cells treated with 10 μM of **L** and Mitotracker deep Red (MTR): **a** Fluorescence imaging of **L** and MTR in HepG2 cells. **b** Correlation

plot of **L** and MitoTracker intensities. **c** Intensity profile of ROIs across HepG2 cells. Scale bar 10 μm

that compound **L** is a promising fluorescent probe for targeting mitochondria.

Conclusion

In summary, an A–D– π –A type red fluorescent compound was designed and synthesized. Compound **L** was almost non-emissive when dissolved in ethanol, but became strongly emissive when aggregated in water solution, demonstrating a typical AIE phenomenon. Confocal imaging experiment indicated that compound **L** was capable of targeting the mitochondrial in living HepG2 cells. Current results offer a platform for the development of new AIE materials with red emission for targeting mitochondria.

Acknowledgements This study was supported by the Science Foundation of Department Education of Anhui Province (KJ2017ZD49), and the Talent Foundation of the Education Department of Anhui (gxb-jZD2016111), Doctoral Startup Foundation of Wannan Medical College (wYRCQD201715).

References

- Chang ZF, Jing LM, Chen B, Zhang MS, Cai XL, Liu JJ, Ye YC, Lou XD, Zhao ZJ, Liu B, Wang JL, Tang BZ (2016) Rational design of asymmetric red fluorescent probes for live cell imaging with high AIE effects and large two-photon absorption cross sections using tunable terminal groups. *Chem Sci* 7:4527–4536. <https://doi.org/10.1039/C5SC04920B>
- Dennington R, Keith T, Millam J (2009) GaussView, version 5. Semi-chem Inc, Shawnee Mission

- Ding D, Li K, Liu B, Tang BZ (2013) Bioprobes based on AIE fluorogens. *Acc Chem Res* 46:2441–2453. <https://doi.org/10.1021/ar3003464>
- Frisch M, Trucks G, Schlegel H, Scuseria G, Robb M, Cheeseman Scalmani, Barone Mennucci B, Petersson G (2009) Gaussian 09, revision A. Gaussian Inc, Wallingford
- Gui C, Zhao EG, Kwok RTK, Leung ACS, Lam JWY, Jiang MJ, Deng HQ, Cai YJ, Zhang WJ, Su HF, Tang BZ (2017) AIE-active theranostic system: selective staining and killing of cancer cells. *Chem Sci* 8:1822–1830. <https://doi.org/10.1039/C6SC04947H>
- Hu QL, Gao M, Feng GX, Liu B (2014) Mitochondria-targeted cancer therapy using a light-up probe with aggregation-induced-emission characteristics. *Angew Chem Int Ed* 53:14225–14229. <https://doi.org/10.1002/anie.201408897>
- Huang YY, Zhang GX, Hu F, Jin YL, Zhao R, Zhang DQ (2016) Emissive nanoparticles from pyridinium-substituted tetraphenylethylene salts: imaging and selective cytotoxicity towards cancer cells in vitro and in vivo by varying counter anions. *Chem Sci* 7:7013–7019. <https://doi.org/10.1039/C6SC02395A>
- Kwork RT, Leung CWT, Lam JWY, Tang BZ (2015) Biosensing by luminogens with aggregation-induced emission characteristics. *Chem Soc Rev* 44:4228–4238. <https://doi.org/10.1039/C4CS00325J>
- Li LQ, Wang LY, Tang H, Cao DR (2017a) A facile synthesis of novel near-infrared pyrrolopyrrole aza-BODIPY luminogens with aggregation-enhanced emission characteristics. *Chem Commun* 53:8352–8355. <https://doi.org/10.1039/C7CC04568A>
- Li XS, Jiang MJ, Lam JWY, Tang BZ, Qu JNY (2017b) Mitochondrial imaging with combined fluorescence and stimulated raman scattering microscopy using a probe of the aggregation-induced emission characteristic. *J Am Chem Soc* 139:17022–17030
- Liu G, Yang MD, Wang LK, Zheng J, Zhou HP, Wu JY, Tian YP (2014) Schiff base derivatives containing heterocycles with aggregation-induced emission and recognition ability. *J Mater Chem C* 2:2684–2691. <https://doi.org/10.1039/C3TC32591A>
- Lu HG, Zheng YD, Zhao XW, Wang LJ, Ma SQ, Han XQ, Xu B, Tian WJ, Gao H (2016) Highly efficient far red/near-infrared solid fluorophores: aggregation-induced emission, intramolecular charge transfer, twisted molecular conformation, and bioimaging applications. *Angew Chem* 128:163–167. <https://doi.org/10.1002/anie.201507031>
- Luo JD, Xie ZL, Lam JWY, Cheng L, Chen HY, Qiu CF, Kwok HS, Zhan XW, Liu YQ, Zhu DB, Tang BZ (2001) Aggregation-induced emission of 1-methyl-1,2,3,4,5-pentaohenylsilole. *Chem Commun*. <https://doi.org/10.1039/B105159H>
- Mei J, Leung NLC, Kwok RTK, Lam JWY, Tang BZ (2015) Aggregation-induced emission: together we shine, united we soar. *Chem Rev* 115:11718–11940. <https://doi.org/10.1021/acs.chemrev.5b00263>
- Thomas SW III, Joly GD, Swager TM (2007) Chemical sensors based on amplifying fluorescent conjugated polymers. *Chem Rev* 107:1339–1386. <https://doi.org/10.1021/cr0501339>
- Tian XH, Hussain S, Wang H, Zhang Q, Zhao M, Chen JY, Zhang H, Zhou HP, Chen Y, Tian YP (2017) A series of water-soluble pyridinium derivatives with two-photon absorption in the near infrared region for mitochondria targeting under stimulated emission depletion (STED) nanoscopy. *Dyes Pigm* 147:90–98. <https://doi.org/10.1016/j.dyepig.2017.07.025>
- Viglianti L, Leung NLC, Xie N, Gu XG, Sung HYH, Miao Q, Williams ID, Licandro E, Tang BZ (2017) Aggregation-induced emission mechanistic study of the clusteroluminescence of tetraethyethene. *Chem Sci* 8:2629–2639. <https://doi.org/10.1039/c6sc05192h>
- Wang XC, Tian XH, Zhang Q, Sun PP, Wu JY, Zhou HP, Jin BK, Yang JX, Zhang SY, Wang CK, Tao XT, Jiang MH, Tian YP (2012) Assembly, two-photon absorption, and bioimaging of living cells of a cuprous cluster. *Chem Mater* 24:954–961. <https://doi.org/10.1021/cm2029855>
- Wang H, Tian XH, Du W, Zhang Q, Guan LJ, Wang AD, Zhang YJ, Wang CK, Zhou HP, Wu JY, Tian YP (2016) A two-photon fluorescent RNA probe screened from a series of oxime-functionalized 2,2':6',2''-terpyridine ZnX₂ (X = Cl, Br, I) complexes. *J Mater Chem B* 4:4818–4825. <https://doi.org/10.1039/C6TB01202G>
- Wang H, Hu L, Du W, Tian XH, Hu ZJ, Zhang Q, Zhou HP, Wu JY, Uvdal K, Tian YP (2018a) Mitochondria-targeted iridium (III) complexes as two-photon fluorogenic probes of cysteine/homocysteine. *Sens Actuators B* 255:408–415. <https://doi.org/10.1016/j.snb.2017.08.074>
- Wang Y, Mao PD, Wu WN, Mao XJ, Fan YC, Zhao XL, Xu ZQ, Xu ZH (2018b) New pyrrole-based single-molecule multianalyte sensor for Cu²⁺, Zn²⁺, and Hg²⁺ and its AIE activity. *Sens Actuators B* 255:3085–3092. <https://doi.org/10.1016/j.snb.2017.09.133>
- Xie HT, Wu YL, Zeng F, Chen JJ, Wu SZ (2017) An AIE-based fluorescent test strip for the portable detection of gaseous phosgene. *Chem Commun* 53:9813–9816. <https://doi.org/10.1039/c7cc05313d>
- Yannai T, Tew DP, Handy NC (2004) A new hybrid exchange-correlation functional using the coulomb-attenuating method (CAM-B3LYP). *Chem Phys Lett* 393:51–57. <https://doi.org/10.1016/j.cplett.2004.06.011>
- Zhang JN, Kang H, Li N, Zhou SM, Sun HM, Yin SW, Zhao N, Tang BZ (2017) Organic solid fluorophores regulated by subtle structure modification: color-tunable and aggregation-induced emission. *Chem Sci* 8:577–582. <https://doi.org/10.1039/C6SC02875F>
- Zheng Z, Yu ZP, Yang MD, Jin F, Zhang Q, Zhou HP, Wu JY, Tian YP (2013) Substituent group variations directing the molecular packing, electronic structure, and aggregation-induced emission property of isophorone derivatives. *J Org Chem* 78:3222–3234. <https://doi.org/10.1021/jo400116j>